Applied Catalysis B: Environmental 150–151 (2014) 305–314

Contents lists available at ScienceDirect

Applied Catalysis B: Environmental

journal homepage: www.elsevier.com/locate/apcatb

Ce-V loaded metal oxides as catalysts for dechlorination of chloronitrophenol by ozone

Suresh Maddila, Venkata D.B.C. Dasireddy, Sreekanth B. Jonnalagadda*

School of Chemistry & Physics, University of KwaZulu-Natal, Westville Campus, Chiltern Hills, Durban 4000, South Africa

ARTICLE INFO

Article history:
Received 8 August 2013
Received in revised form
17 December 2013
Accepted 19 December 2013
Available online 28 December 2013

Keywords:
Chloronitrophenol
Dihydroxyhexadienedioic acid
Ozone
Cerium
Vanadium

ABSTRACT

We report the catalytic degradation of chloronitrophenol (CNP) facilitated by ozone using cerium-vanadium oxide loaded on metal oxides supports alumina and silica as catalysts. The catalyzed ozonation markedly accelerated the degradation of CNP. Catalyst materials were synthesized and characterized by using various surface characterization techniques including XRD, BET, TPD, ICP, SEM, TEM and FT-IR. The influences of hydroxyl radical scavengers, pH values, and reaction products on degradation were investigated. Alkaline pH facilitated and accelerated the generation of hydroxyl radicals by the heterogeneous catalyst. The oxidation products formed in the reaction were characterized by ^{1}H NMR and LC–MS mass spectral data. 3,4-Dihydroxyhexa-2,4-dienedioic acid (DDA), 2-hydroxymaleic acid (HMA) and oxalic acid (OA) were the main oxidation products. 5% Ce-V/SiO_2 proved to be economical and feasible choice for catalytic ozonation and dechlorination of CNP in water.

1. Introduction

Chlorinated organic compounds have applications in multiple fields and can found in nearly all major environmental compartments [1]. Chloronitrophenols are one of the most commonly found compounds in the wastes from many industries including pesticides, pharmaceuticals, organic chemicals manufacturing, petroleum refining, petrochemicals, paints, resins, plastics and as a dye intermediates [2]. Even trace quantities of the chloronitrophenol derivatives are highly toxic, mutagenic, carcinogenic [3]. Furthermore, they can persist for many years in the environment because of their resistance to microbiological degradation [4–6]. Due to their toxicity and persistence, their polluting effects on our eco-system results in potential health risk to humans. This raises an urgent need for efficient dechlorination methods to eliminate chloro, nitro functionalities from both concentrated and diluted industrial effluents which pollute the ground water [7].

Worldwide, ozone is extensively used in water treatment technology because of its high oxidation and disinfection potential, for example in decoloration and in elimination of refractory pollutants [8,9]. It is now widely assumed that ozone reacts in aqueous solution on various organic and inorganic compounds, either by a direct reaction of molecular ozone or through a radical type reaction involving $^-$OH induced by the ozone decomposition in water. While, the reaction by molecular ozone is selective, attack by hydroxyl radicals is less selective [10,11].

Generally simple ozonation (O_3) is ineffective for oxidizing some organic contaminants due to its selective reactions at acidic and neutral pH conditions [12]. Studies in recent years using advanced oxidation processes (AOPs) shown that the effective removal of many organic compounds from the aqueous medium can be successfully achieved [13–15]. For this reason, more attention was paid to advanced oxidation processes to improve the destruction of recalcitrant organic pollutants possibly by enhanced hydroxyl radical generation [16]. AOPs are initiated by a radical reaction using different conditions such as alkaline solution (O_3/$^-$OH), photolysis of ozone (O_3/UV), per ozone (O_3/H_2O_2), catalytic ozonation and combination between them [17,18]. Catalyzed ozonation, in particular has been recognized as an efficient process to achieve the oxidation and degradation of toxic organic compounds.

In recent years, heterogeneous catalytic ozonation has received much attention in water treatment due to its potential and effectiveness in the degradation and mineralization of refractory organic pollutants and minimal destructive effect on water quality [12,16,18]. Several researches have been reported on the degradation of chlorophenols in aqueous solution by the heterogeneous catalytic ozonation processes, but very few reports on reactions of nitrochlorophenols [19–21]. In this study, we report the results of

* Corresponding author. Tel.: +27 31 260 7325; fax: +27 31 260 3091.
E-mail address: jonnalagaddas@ukzn.ac.za (S.B. Jonnalagadda).

0926-3373/$ – see front matter © 2014 Elsevier B.V. All rights reserved.
http://dx.doi.org/10.1016/j.apcatb.2013.12.036

elimination of chloro and nitro groups from 4-chloro-2-nitrophenol and the effect of catalyst loading on the support and their reaction mechanism.

2. Materials and methods

2.1. Preparation of catalysts

The wet impregnation method was used in the preparation of metal oxide supported catalysts [22–24]. The catalysts were prepared by wet impregnation method by dissolving appropriate amount of Ce (Cerium nitrate, Aldrich-99%) and V (Vanadyl sulfate, Aldrich-99%) with a ratio of 1:1 in distilled water (50.0 mL) and adding it to 5 g of γ-alumina (γ-Al_2O_3, Aldrich) or Silica (SiO_2, Aldrich). The mixture is stirred for 3 h using a magnetic stirrer at room temperature and left at room temperature for overnight. Catalysts are further dried in an oven at 130–140 °C for 12 h and calcined in the presence of air, at 550 °C for 3 h to obtain the 1%, 2.5% and 5% (w/w) of Ce-V supported catalysts.

2.2. Instrumentation

2.2.1. Characterization of catalysts

2.2.1.1. Textural properties. The Brunauer–Emmett–Teller (BET) surface area, total pore volume and average pore size were measured using a Micrometrics Tristar II surface area and porosity analyser. Prior to the analysis, the powdered samples (~0.180 g) were degassed under N_2 for 12 h at 200 °C using a Micromeritics FlowPrep 060 instrument. Textural properties of catalyst samples were measured by N_2 adsorption–desorption isotherms obtained at −196 °C.

2.2.1.2. Inductively coupled plasma-optical emission spectroscopy (ICP-OES). The actual metal loading was determined by using Perkin Elmer Inductively coupled plasma Optical Emission Spectrometer (ICP-OES) Optima 5300 DV. Samples were solubilized in aqua regia and homogenized by a microwave digestion process, prior to ICP analysis.

2.2.1.3. Temperature programmed desorption (TPD). In the TPD experiments, the catalyst was pretreated at 350 °C under the stream of helium for 60 min. The temperature was then decreased to 80 °C. A mixture of 5% ammonia in helium was passed over the catalyst at a flow rate of 30 mL/min for 60 min. The excess ammonia was removed by purging with helium for 30 min. The temperature was then raised gradually to 950 °C by ramping at 10 °C min^{-1} under the flow of helium and desorption data was recorded.

2.2.1.4. X-ray diffraction (XRD) analysis. Different metal oxide phases in the catalysts were observed using powder X-ray diffraction (XRD) performed on a Bruker D8 Advance instrument, equipped with an Anton Paar XRK 900 reaction chamber, a TCU 750 temperature control unit and a CuKα radiation source with a wavelength of 1.5406 nm at 40 kV and 40 mA. Diffractograms were recorded over the range 15–90° with a step size of 0.5 per second.

2.2.1.5. FT-IR analysis. FT-IR spectra of various catalyst samples were recorded on a Nicolet Impact 400 equipment and Nicolet Impact Model-420 spectrometer with a 4 cm^{-1} resolution and 128 scans in the mid IR (400–4000 cm^{-1}) region using the KBr pellet technique. About 100.0 mg of dry KBr was mixed with a little amount (10.0 mg) of the sample and was ground for homogenization. During the mixing an IR lamp was used for drying. The mixture was then pressed into a transparent, thin pellet at 10 ton cm^{-2}. These pellets were used for the IR spectral measurements.

2.2.1.6. Electron microscopy analysis (SEM & TEM). The Transmission Electron Microscopy (TEM) images were viewed on a Jeol JEM-1010 electron microscope. The images were captured and analyzed by using iTEM software. High resolution TEM images were recorded by using Jeol JEM 2100 Electron Microscope. The Scanning Electron Microscopy (SEM) measurements were carried out using a JEOL JSM-6100 microscope equipped with an energy-dispersive X-ray analyzer (EDX). The images were taken with an emission current = 100 μA by a Tungsten (W) filament and an accelerator voltage = 12 kV. The catalysts were secured onto brass stubs with carbon conductive tape, sputter coated with gold and viewed in JEOL JSM-6100 microscope. The pre-treatment of the samples consisted of coating with an evaporated Au film in a Polaron SC 500 Sputter Coater metallizator to increase the catalyst electric conductivity.

2.2.2. Characterization of the products

2.2.2.1. GC–MS analysis. The GC–MS analysis was carried out in EI mode and the spectra were recorded in the interval 35–500 amu. For analysis of compounds, Agilent 6890 gas chromatograph equipped with a quadruple Agilent 5973n mass selective detector was used. Column specifications: J&W DB5MS, 30 m length, 250 μm diameter and 0.25 μm film thickness. The temperature program used during the GC–MS analysis was ramped as follows: 50 °C (2 min), 30 °C min^{-1} until 300 °C (10 min). The sample was carried out with a 1.50 min splitless time at 250 °C. The carrier used was helium.

2.2.2.2. ^1H NMR & LC–MS. ^1H NMR (400 MHz) spectra were recorded on a Bruker AMX 400 MHz NMR spectrometer in $CDCl_3$/DMSO-d_6 solution using TMS as an internal standard. All chemical shifts are reported in δ (ppm) using TMS as an internal standard. The mass spectra were recorded on an Agilent 1100 LC/MSD instrument, with method API-ES, at 70 eV.

3. Results and discussion

3.1. Ozonolysis experiment

Ozone was generated using a Fischer Ozone 500 generator, which produced ozone by the electric discharge of oxygen from a compressed oxygen cylinder via the corona discharge method. All ozone aeration experiments were carried out in a system elaborated by Pullabhotla et al. [22–24]. All the ozone aeration experiments were carried out under the controlled conditions of room temperature (20 ± 1) °C using 25 mL 10% (w/v) of 4-chloro-3-nitrophenol (CNP) in water at fixed ozone concentration (0.05 M) and flow rate of 100 ml/min for 5 h. Fig. 1 illustrates the dimensions of the semi-batch reactor used. Ozone gas was bubbled into a 50 cm^3 reactor through a sintered porous diffuser. A magnetic stirrer placed at the bottom of the reaction vessel was used to ensure maximum contact of the substrate with ozone by continuous stirring. The amount of ozone was estimated by volumetric method trapping it in KI solution and titrating the liberated iodine using standard thiosulfate solution with starch as indicator [24]. Flow rates and ozone concentrations were calibrated and highly reproducible. Parameters were checked in duplicate runs, prior to and after each of the experiments. Results were highly reproducible and with less than 5% difference. Where difference was greater, such experiments replicated and data with less than 5% differences were only considered. As most of the experiments were done only in duplication, statistical analysis of the results could not be undertaken. In all cases although differences were small, trends were consistent, hence cautions approach is taken while comparing the results.

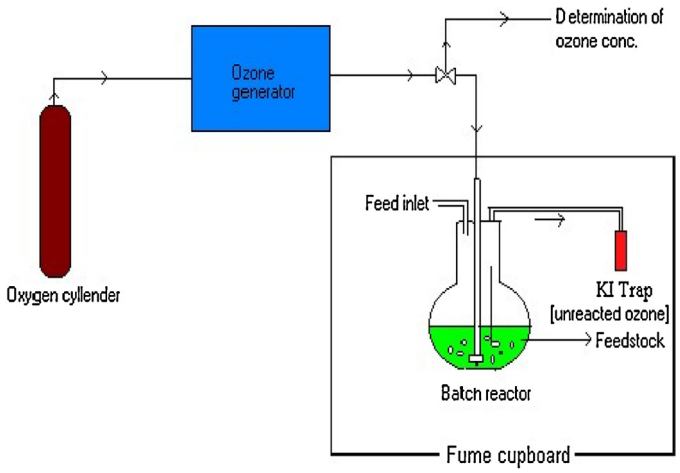

Fig. 1. Dimensions of reactor used in ozonation reactions.

3.2. Catalyst testing and product identification

All the ozonation experiments were showed by exposing the samples with ozone enhanced with oxygen for different times. No reaction occurred with oxygen alone. After ozone aeration, the organic portion of the reaction mixture was extracted and analyzed after every reaction with 60 min intervals. Three products were separated and identified by GC–MS (Fig. 2). The peaks from 9.5 to 12.75 retention times refer to the different carboxylic acid compounds formed due to the further oxidation of the main products of the reaction. The peaks at retention time 9.55, 9.84 refer to the first products of oxalic acid (OA), 2-hydroxymaleic acid (HMA). Further, the reacted 3,4-dihydroxyhexa-2,4-dienedioic acid (DDA) from the chromatogram is confirmed by injecting the substrate, which elutes at the retention time 12.51. Based on the mass spectra and the reference standards, the first oxidation products were confirmed to be 3,4-dihydroxyhexa-2,4-dienedioic acid (DDA) and the second products were 2-hydroxymaleic acid (HMA) and Oxalic acid (OA). The ^{1}H NMR spectrum of DDA showed broad singlet protons for the 2COOH group at δ 12.89 ppm and

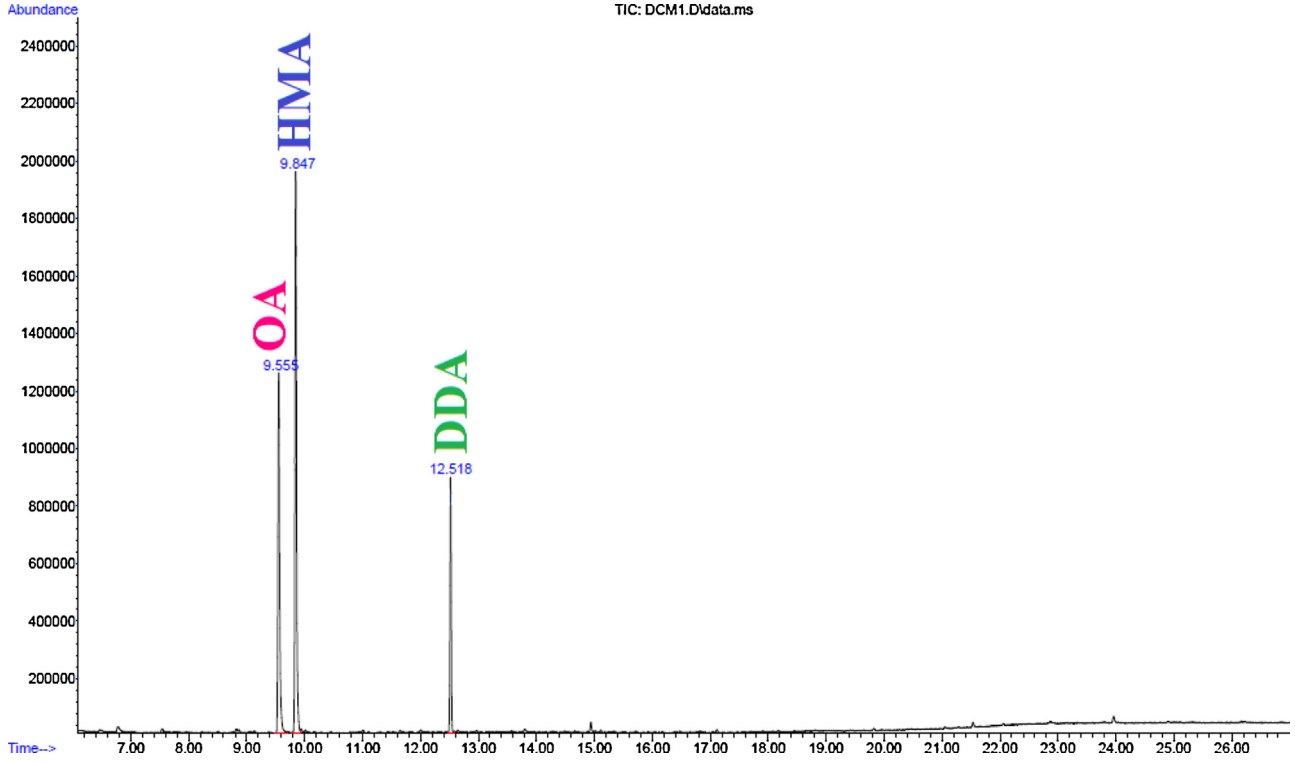

Fig. 2. GC–MS chromatogram of product mixture.

Table 1
BET surface area, TPD data and Elemental analysis of Ce-V loaded supports.

Catalyst	Surface area (m^2/g)	Pore volume (cm^3/g)	Pore size (A°)	ICP (wt%)		Acidity (mmol NH_3/g)	Specific acidity (mmol NH_3/m^2)	EDX (wt%)	
				Ce	V			Ce	V
SiO_2	210	0.75	189	–	–	3749	17.7	–	–
1% Ce-V/SiO_2	223	0.97	172	0.47	0.48	3853	17.2	0.45	0.44
2.5% Ce-V/SiO_2	217	0.91	168	1.25	1.24	3946	18.1	1.19	1.22
5% Ce-V/SiO_2	211	0.86	162	2.48	2.49	4125	19.5	2.43	2.41
Al_2O_3	251	0.98	125	–	–	850	3.4	–	–
1% Ce-V/Al_2O_3	207	0.58	92	0.48	0.49	963	4.7	0.43	0.46
2.5% Ce-V/Al_2O_3	198	0.53	90	1.24	1.23	1025	5.8	1.20	1.18
5% Ce-V/Al_2O_3	177	0.49	93	2.50	2.48	1258	7.2	2.41	2.41

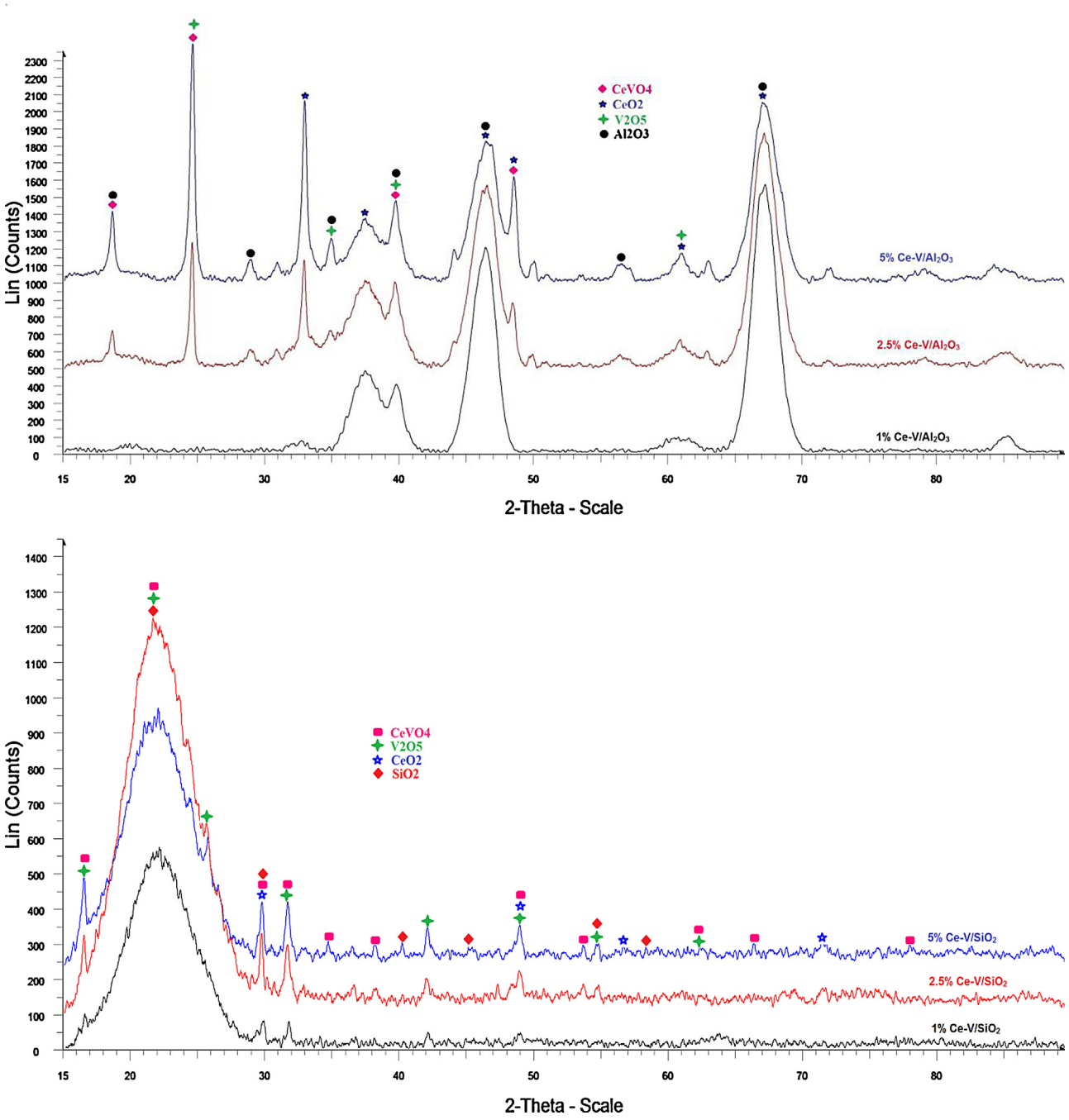

Fig. 3. XRD spectra: (a) 1%, 2.5% & 5% Ce-V loaded on Al_2O_3; (b) 1%, 2.5% & 5% Ce-V loaded on SiO_2; (c) 2.5% Ce-V on Al_2O_3; (d) 2.5% Ce-V on SiO_2; (e) 5% Ce-V on Al_2O_3; (f) 1% Ce-V on SiO_2.

singlet at δ 8.01 ppm for the 2OH group, respectively (Supplementary Materials Fig. 1a). The LC–MS mass spectrum showed m/z peak at 173 (M−H) (Supplementary Materials Fig. 1b). Similarly compound HMA displayed a broad singlet at δ 13.86 ppm for 2COOH protons, two singlet protons showed at 8.45, 6.91 ppm for OH, CH groups (Supplementary Materials Fig. 2a). Moreover, the LC–MS mass spectrum showed at m/z at 132 (M^+) (Supplementary Materials Fig. 2b). The functional groups observed in the ^1H NMR and LC–MS spectrum were in good agreement with spectra corresponding to DHHDA and HMA. Further, the qualitative test (lime water) confirmed the release of CO_2 during the ozonation reaction and suggested some mineralization of CNP. Ozonation of organic compounds in water is known to produce more biodegradable oxygenated organic products and low molecular weight acids.

3.3. BET surface area and elemental analysis (BET & ICP)

The surface areas and the elemental composition for the catalysts are shown in Table 1. The texture of the catalysts was dependent on the Ce-V wt% loading and the higher loading i.e. 5% Ce-V resulted in a significant decrease in the surface area as well as the pore volume. This could be attributed to the blocking of the narrow pores of the support with the active component making it inaccessible to nitrogen molecules (Supplementary Materials Fig. 3). Table 1 shows the nitrogen adsorption–desorption

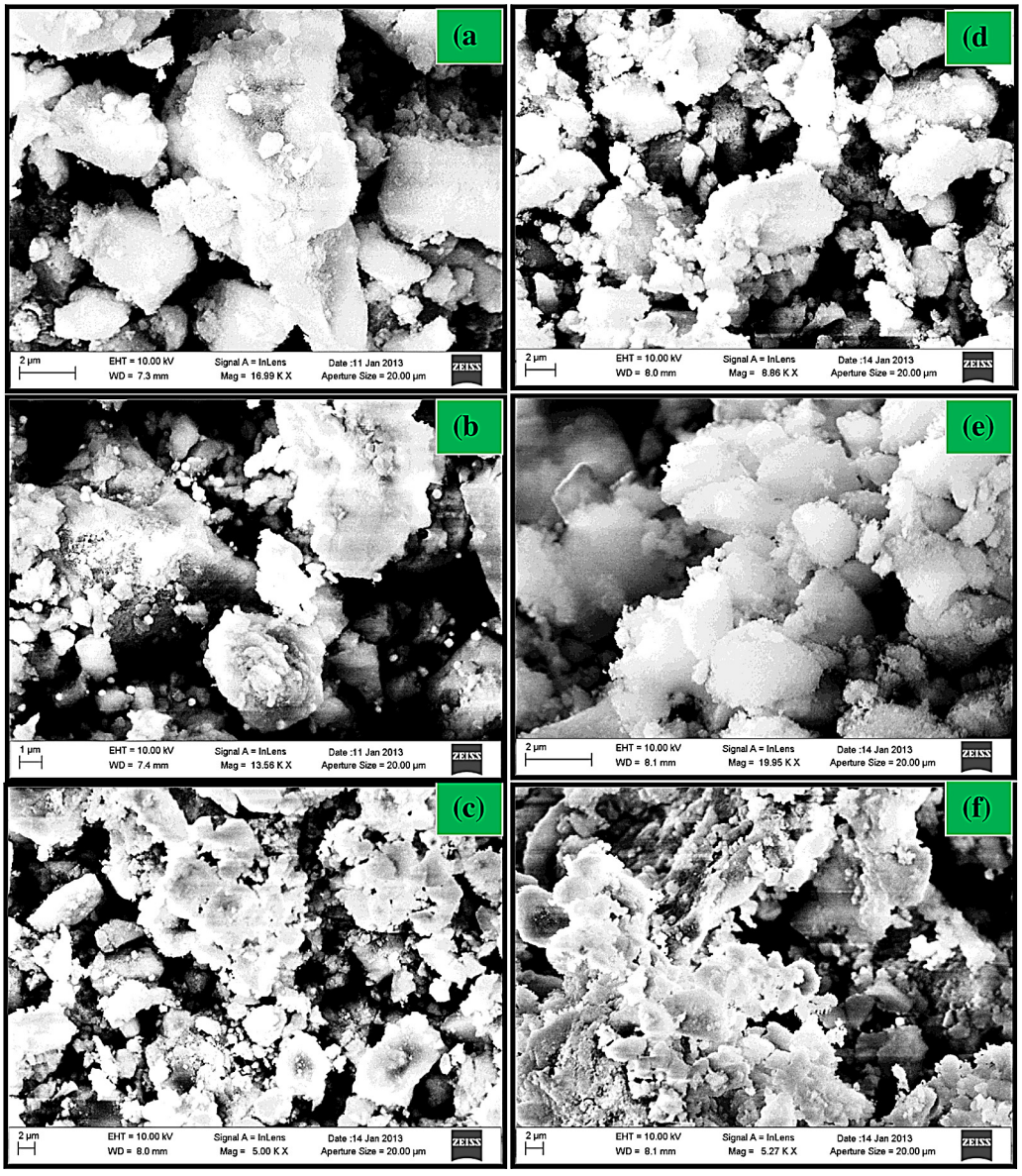

Fig. 4. SEM images: (a) 1% Ce-V on Al_2O_3; (b) 1% Ce-V on SiO_2;.

isotherms for the Ce-V supported on alumina and silica catalysts. All the catalysts showed a similar pattern in adsorption–desorption isotherms and all the catalysts display the characteristic hysteresis loop of a type-IV isotherm (IUPAC) lying in the p/p° range of 0.7–0.85, demonstrating mesoporous character (Table 1). An inflection observed between the p/p° range of 0.80–0.95 may be attributed to the macropores caused by Ce-V particle–particle porosity. The catalysts also exhibit a step increase at this relative pressure range due to the filling of interparticle macropores of the catalyst with the nitrogen. The isotherms and average pore sizes remained substantially the same over the range of Ce-V concentration which means that the Ce-V species did not disturb the pore structure of the supports. Ce-V loaded on Al_2O_3 support material exhibited a lower surface area than silica supported catalysts. Surface area decreased with 5% loading of Ce-V on both alumina and silica. The silica and alumina have higher BET surface area and with 1 wt% Ce-V loading. When the Ce-V wt% loading to 5% all the pores occupied by Ce-V and forming layers on the surface of metal supports and decreases the total surface area. The loading of Ce-V on silica also exhibited decrease in surface area. Also during the impregnation stage in the preparation, surface hydroxyl groups of the silica get consumed by reaction with the active phase precursor. Such a surface reaction may be caused the decrease of surface area.

3.4. Temperature programmed desorption

From the TPD experiments, it is evidenced that the Ce-V increases the acidic nature of the supports which is also recorded by increases of specific acidity (Table 1). Ce-V, which is strong acidic metals, with interaction with the acidic sites on the surface of the supports, i.e., silica, and alumina increases their surface acidity. With silica acidic by nature, among all the catalysts, Ce-V supported on silica catalysts showed high acidity and specific acidity. Further, the increase in the acidic nature is high with silica relative to the other supports with Ce-V loading. Thus the Ce-V loading is effecting mainly the Brønsted acidic sites (strong acidic) on the silica surface, but not diminishing the Lewis acidic sites (Weak acidic sites). Thus,

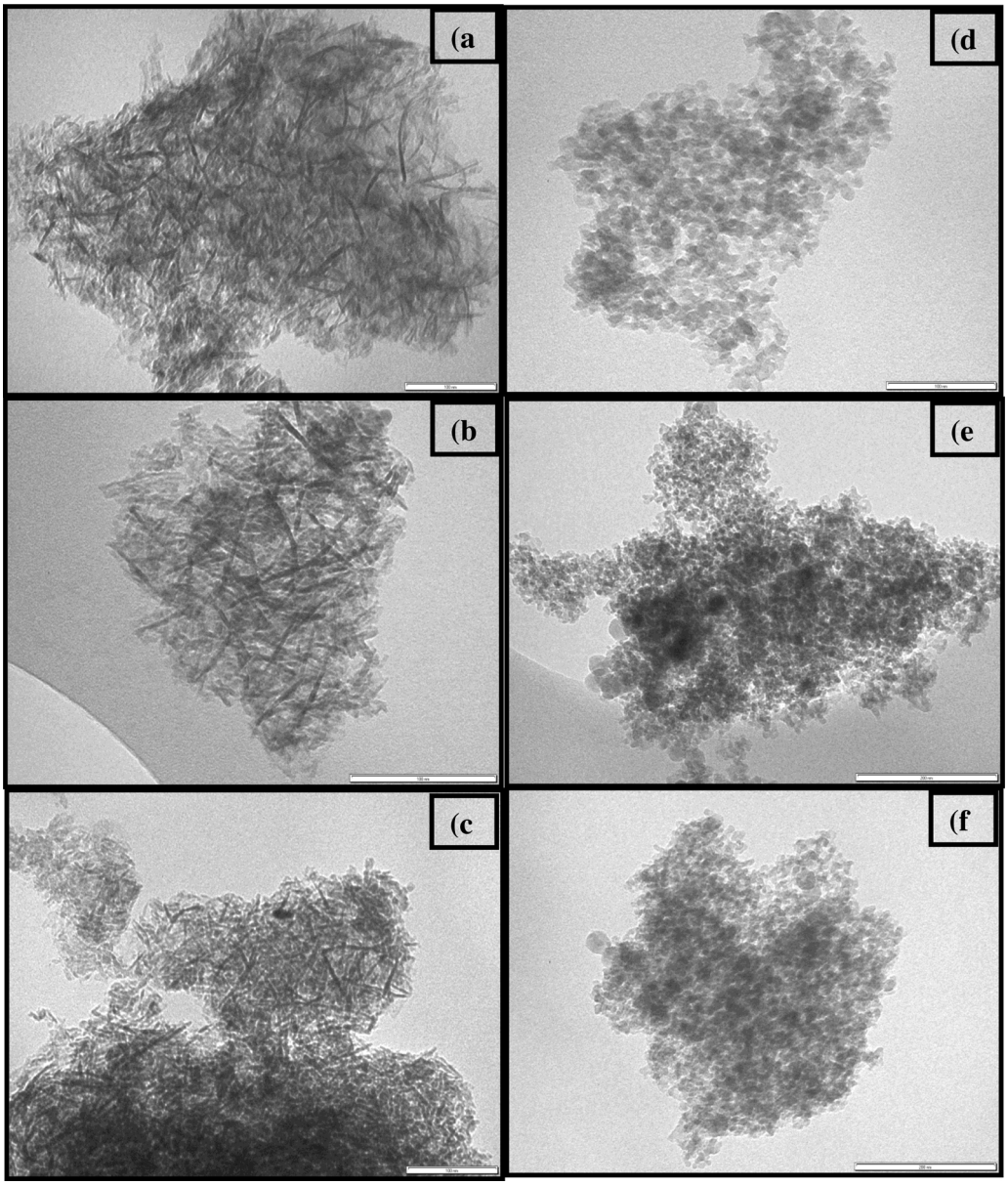

Fig. 5. TEM images: (a) 1% Ce-V on Al_2O_3; (b) 1% Ce-V on SiO_2; (c) 2.5% Ce-V on Al_2O_3; (d) 2.5% Ce-V on SiO_2; (e) 5% Ce-V on Al_2O_3; (f) 1% Ce-V on SiO_2.

by comparison of increase in the ratio of the acidity, we can perceive that Ce-V is increasing the Brønsted acidic sties of the silica and alumina.

3.5. X-ray diffraction (XRD)

Fig. 3a (1%, 2.5% & 5% Ce-V/Al_2O_3), Fig. 3b (1%, 2.5% & 5% Ce-V/SiO_2) shows the XRD patterns of all catalysts. The mixed oxide indicates the $CeVO_4$ phase according to JCPDS12-757, samples show sharp diffraction peaks at $2\theta = 22.1^\circ$, 29.6°, 32°, 39.2°, 49.7°, and 54°. As can be seen from the both figures, the vanadium oxide, samples show sharp diffraction peaks at $2\theta = 17.4^\circ$, 26°, 42.2°, 49°, and 62.4° (JCPDS41-1426). All the peaks of CeO_2 sample in the XRD spectra shows sharp diffraction peaks at $2\theta = 29.8^\circ$, 32.5°, 37.2°, 46.2°, 49.1°, 67.1°, and 72.4° (JCPDS-34-0394).

3.6. Electron microscopy analysis (SEM & TEM)

Fig. 4a–f displays SEM micrographs images of the mixed oxide (CeV) and of the cerium and vanadium oxides samples. These pictures show significant textural and morphological differences of the mixed oxide and the isolated CeO_2 and V_2O_5 oxides. The SEM images of all samples revealed typical spherical type agglomerates with varying sizes within the nanometer range. In particular, no big difference among various samples was noted from these images. Fig. 5a–f shows the TEM micrographs of Ce-V loaded on the supports (Al_2O_3 and SiO_2). Ce-V/Al_2O_3 reveals an aggregate of spherical and needle-like shapes of various sizes, with an increase in the coating of the needle by the spherical materials as the percentage of the dopants increased from 1% Ce-V to 5% Ce-V (Fig. 5a, c and e). Ce-V/SiO_2 also exhibited same aggregated structure as Ce-V/Al_2O_3, but differ in shapes. Ce-V/SiO_2

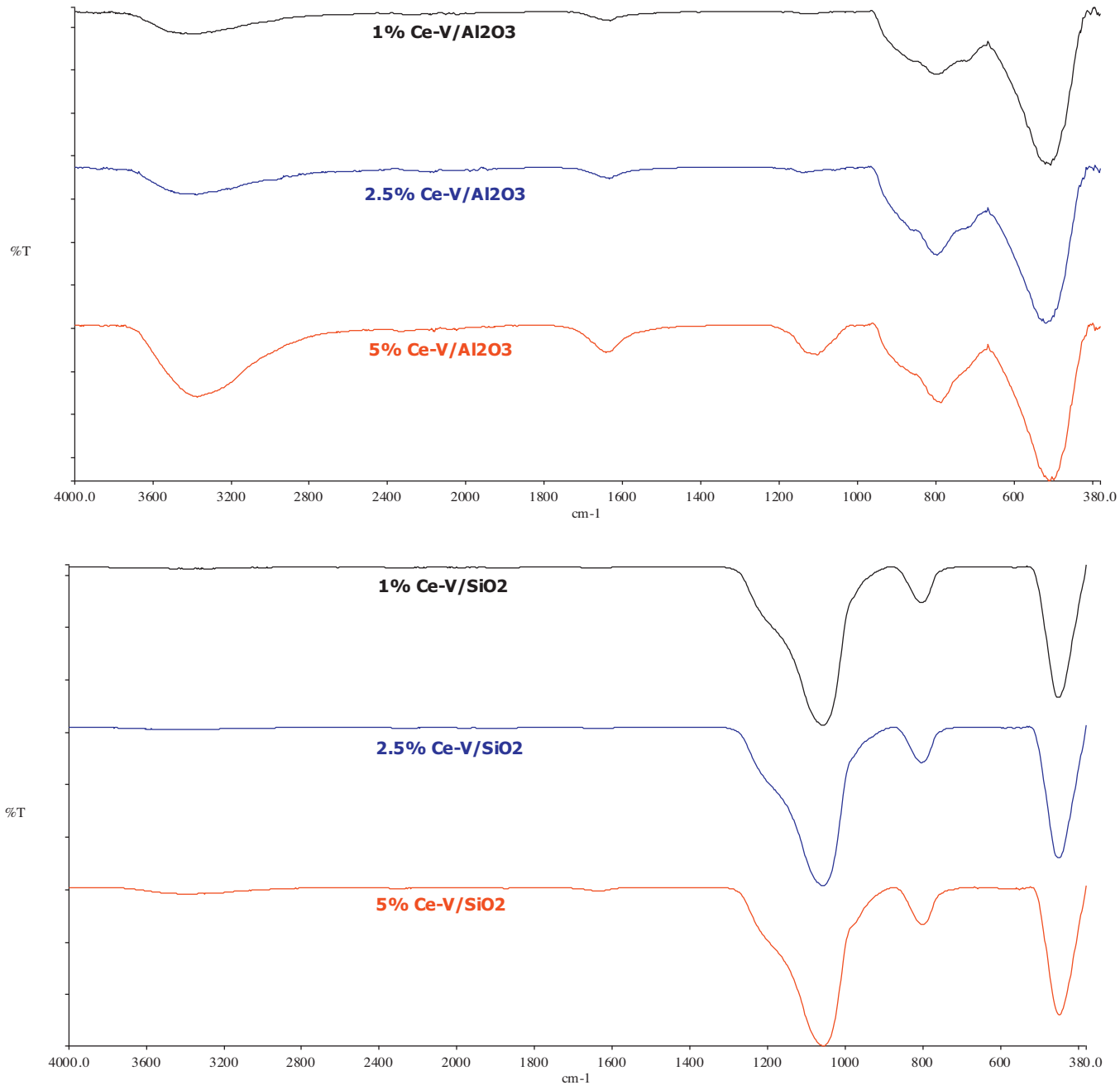

Fig. 6. FT-IR spectra (a) 1%, 2.5% & 5% Ce-V loaded on Al_2O_3; (b) 1%, 2.5% & 5% Ce-V loaded on SiO_2.

possesses spherical shape with various sizes (Fig. 5b, d and f). SEM micrographs Fig. 5a–f, agrees with the micrographs for TEM regarding how aggregated the materials are, with inter-particle voids.

3.7. Fourier transform infrared spectroscopy (FT-IR)

The FTIR spectra of the calcined mesoporous Ce-V/Al_2O_3 and Ce-V/SiO_2 composites are recorded in the spectral range of 4000–400 cm^{-1}. The FTIR spectra of Ce-V/Al_2O_3/SiO_2 for all samples are shown in Fig. 6a and b. The residual water is noticed with a large broad band on the surface of the catalysts (1%, 2.5% & 5% Ce-V/Al_2O_3) around at 3408–3398 cm^{-1}, due to O—H stretching frequency, and broad bands at 1628–1640 cm^{-1} due to the bending vibrations of associated water. The Al_2O_3 peaks are overlapping with the Ce-V-O vibrational stretching arising from the presence of Ce-V oxides. A distinct IR absorption bands at 799, 800 and 793 cm^{-1} observed with 1%, 2.5% & 5% Ce-V/Al_2O_3 [25–27]. The spectra's show a sharp peak at 517, 520 and 512 cm^{-1} indicating Ce-O asymmetric stretching vibrations for 1%, 2.5% and 5% Ce-V/Al_2O_3 respectively. The FT-IR spectrum of 1%, 2.5% & 5% Ce-V/SiO_2 shows absorption bands at 1626, 1630 and 1636 cm^{-1} are attributed to Ce-V-O peaks, sharp vibrational stretching peaks at 452, 450 and 448 cm^{-1} are also due to the presence of Ce-O group [26]. The sharp bands observed at 805, 804 and 802 cm^{-1} due to Ce-V-Si-O group for 1%, 2.5% & 5% Ce-V/SiO_2, respectively. The spectrum shows broad bands due to tetrahedral framework stretching vibrations of Si-O-Si linkages at 1061, 1064 and 1060 cm^{-1}. Very weak bands

at 3391, 3394 and 3392 cm^{-1} are attributed with acidic bridging hydroxyl groups, respectively [22,28].

3.8. Effect of pH

The pH is an important factor in ozone initiated oxidations. The ozonation process at acidic, neutral and alkaline pH medium mainly takes place through the direct oxidation of specific functional groups by molecular ozone, which reacts selectively. The formation in which organic compounds are present, the decomposition of the ozone, and the conversion of the catalyst, are all influenced by pH [12]. To optimize the pH of the reaction, ozonation experiments were conducted with 10% (w/v) of chloronitrophenol, at pH 3, 7 and 11 in presence of 1%, 2.5% and 5% Ce-V oxides on the alumina and silica supports. Similarly, uncatalysed ozonation was also conducted at acidic, neutral and alkaline pH conditions (Fig. 7). Uncatalysed reactions showed improved conversions with increasing pH, which suggests that hydroxyl radicals facilitated the oxidation under alkaline conditions [12,17,23,28]. A perusal of % conversion data in Fig. 7 indicates that like the uncatalysed reaction, the optimum pH for CNP degradation for all bimetallic doped catalysts is pH 11, as the reaction under acidic and neutral conditions showed lower conversions. Observed enhanced reaction under alkaline conditions suggests that increased hydroxyl radical formation and higher pH significantly influenced the surface properties of catalysts and especially the active sites on the surface in catalyzed ozonation process [12,17,22,23,28]. Most of the 5% bimetallic doped catalysts showed 100% conversion in 4 h ozonation time. Fig. 8 also shows the data for % conversion of CNP and selectivity towards products over Ce-V oxides with varing alumina & silica support at pH 11. The obtained results indicate that basic pH provides optimal conditions for both the ozone decomposition and for catalyst activity.

3.9. Effect of metal oxides on supports

An observation of the results in Table 1 shows that the acidic nature of these catalysts is influenced by the metal loading on the support. The increase in metal loading on the support increased the acidity of surface which accelerated the conversion of CNP. As illustrated in Fig. 8, the 5% Ce-V/SiO_2 showed high conversion of CNP due to its high acidic nature. The trend of conversion is in agreement with the acidic sites present on the catalyst (Table 1). The Ce-V/Al_2O_3 catalysts showed low conversion of CNP with compared to Ce-V/SiO_2 catalysts which showed low specific acidity and strength of the acidic sites, i.e. the selectivity towards products is also influenced by the metal loading & the acidity of the catalyst. The catalysts with high acidity (i.e. Ce-V/SiO_2) showed the high selectivity, towards DDA & HMA relative to the catalysts with lower acidity (i.e. Ce-V/Al_2O_3). Thus the metal loading and the acidity of the catalysts have greater influence on the conversion and selectivity towards the products of CNP.

4. Mechanism

Preparation of the catalysts, the structure and dispersion of the catalysts are affected by the preparation method, so good catalyst preparation process can significantly contributes to the catalytic activity. Oxide supports including Al_2O_3, SiO_2, TiO_2 loaded with active components Ce, Zr, Cs, Zn, V, Ni etc. as catalysts of ozone initiated oxidations have been reported in past [17,22,23,28]. The results suggest that the supported catalysts exhibit excellent activity during the ozone decomposition. The catalytic activity of the catalysts mentioned is mainly based on the catalytic

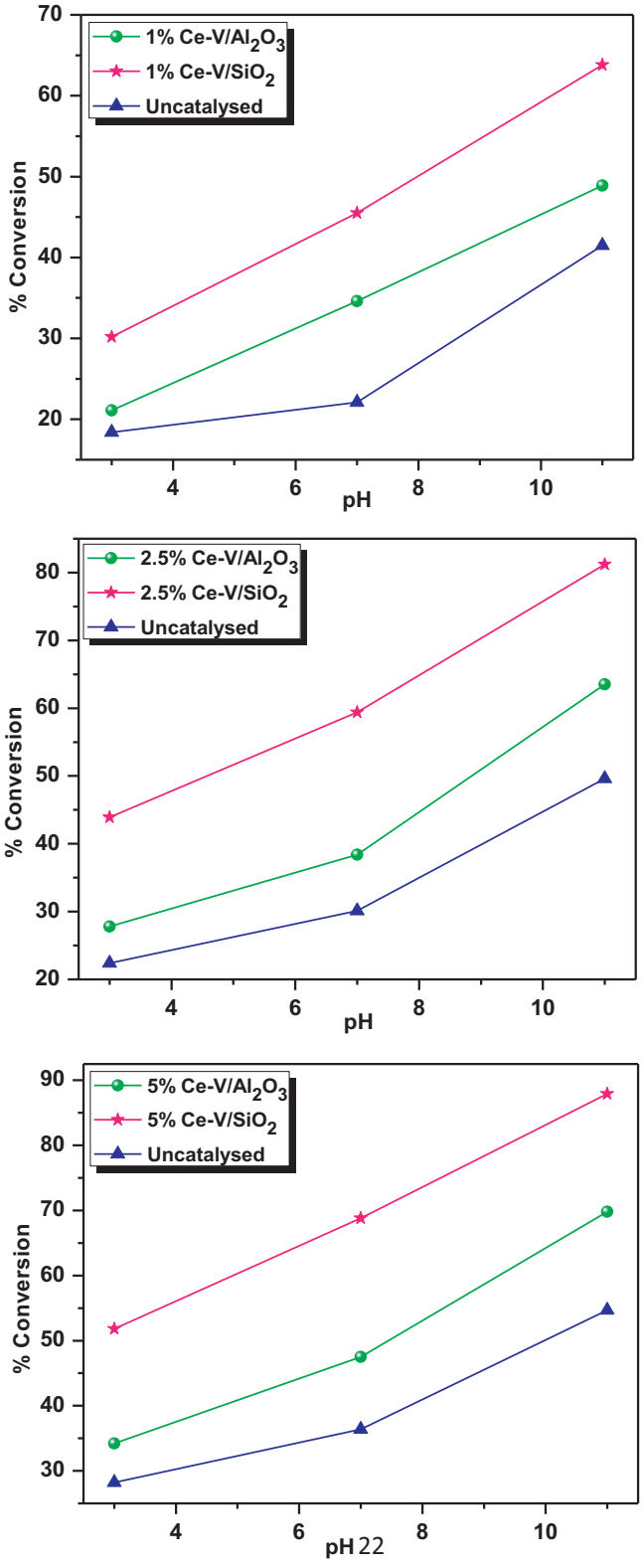

Fig. 7. % conversion of CNP ozonation with different pH.

decomposition of ozone and the enhanced generation of hydroxyl radicals, hydroxyl ions. The efficiency of the catalyzed ozonation process to a great extent depends on the catalyst and its surface properties. pH of the solution is the other important parameter that influences the properties of the surface active sites and ozone decomposition. The modified surface properties of the catalyst due

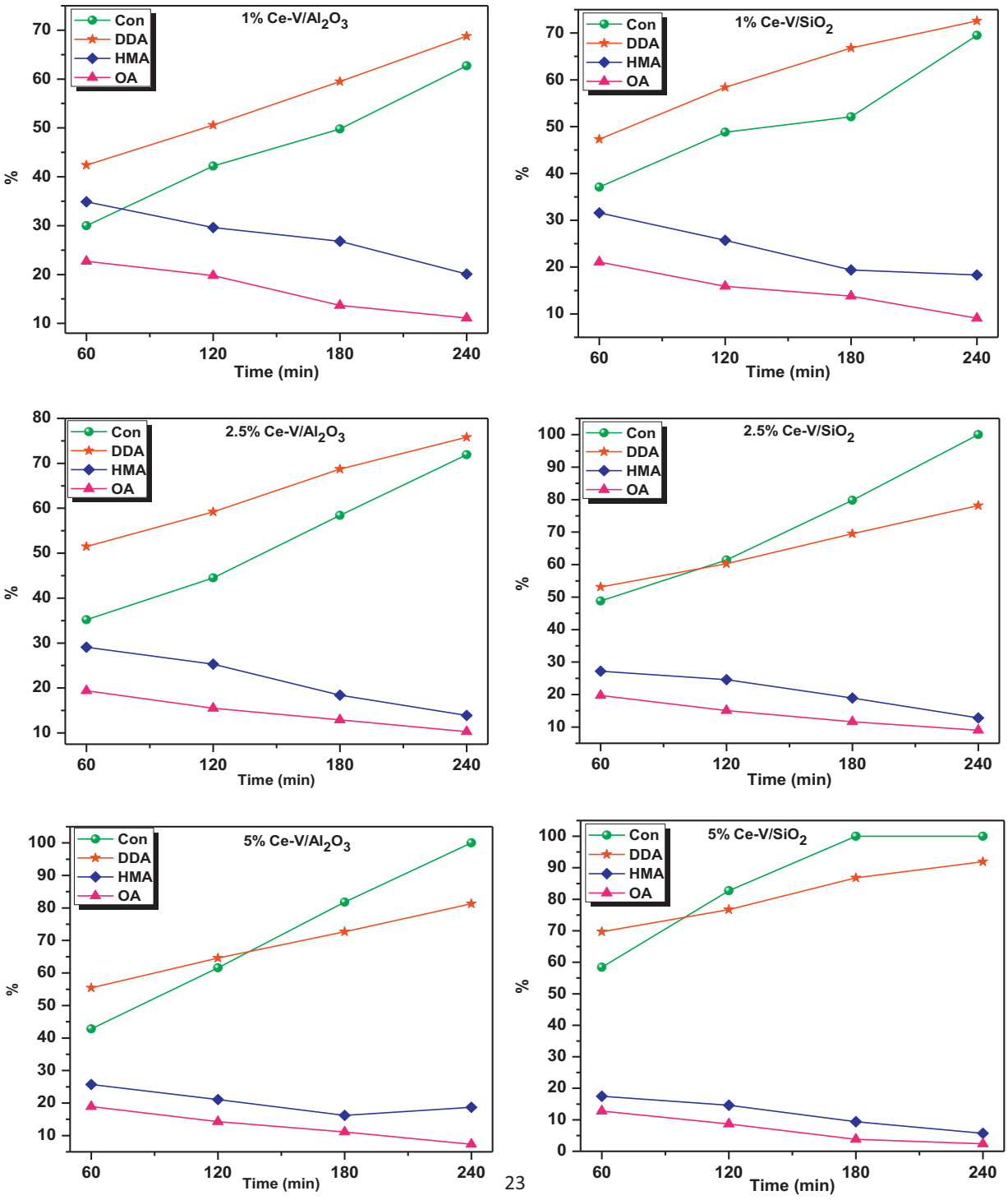

Fig. 8. The conversion and selectivity with 1%, 2.5% & 5% loadings of Ce-V on metal oxides.

to the loading of the Ce-V, facilitates the interaction of surface active sites with every functional group of the organic molecules (both electron withdrawing and donating) enhancing the selective attack the molecular ozone or hydroxyl radicals [29–33].

This phenomenon could be evidenced by the cleavage of the nitro group from aromatic compound. In chloronitro substituted aromatic compounds, because nitro group is a very good leaving group, it can be easily eliminated (denitration) resulting in formation of phenol radicals. Phenol radicals get transformed to phenol through further attack by •OH. The transient intermediate, chlorodihydoxyhexanoic acid, favouring the electrophilic substitution of •OH at the chloro position, the primary stable intermediate DDA is formed, via dechlorination. Further oxidation of DDA by •OH lead to oxygenated aliphatic compounds and formation of degraded to aliphatic carboxylic acids. Maleic acid and oxalic acid were identified in this study. Finally, oxidation of maleic and oxalic acids leads to complete mineralization to CO_2 and H_2O (Scheme 1).

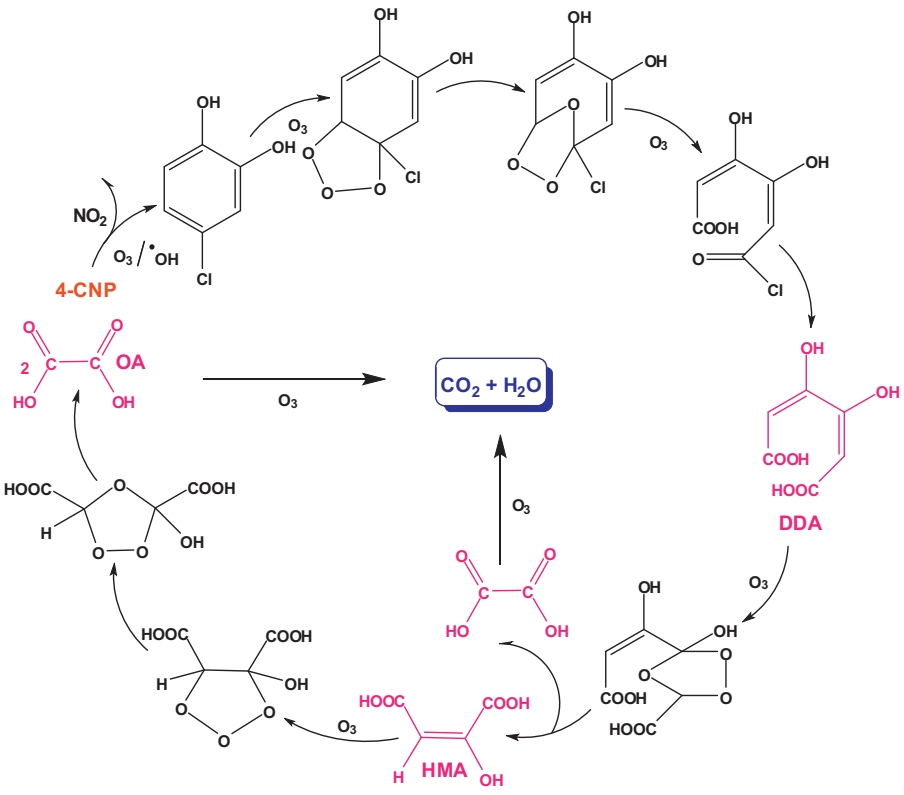

Scheme 1. Mechanism of the scheme.

5. Conclusions

Our study showed that the wet impregnation method permits the synthesis of bi-metallic catalysts with good metal dispersion. The size of catalyst particles and reaction parameters play a significant role in ozonolysis. The CNP oxidation was quantitative. While 3,4-dihydroxyhexa-2,4-dienedioic acid (DDA) is the primary product, 2-hydroxymaleic acid (HMA) and oxalic acid (OA) are the secondary oxidation products and mineralization occurs at tertiary level. All the reactions products were dechlorinated The degradation rate of CNP was significantly enhanced by the 5% Ce-V/SiO_2 catalyzed ozonation and it proved to be an efficient method to eliminate chloro, nitro and hydroxy functionalities from toxic organics in waters.

Acknowledgements

Authors thank the University of KwaZulu-Natal for the financial support and other research facilities for access to the facilities used for the research.

Appendix A. Supplementary data

Supplementary data associated with this article can be found, in the online version, at http://dx.doi.org/10.1016/j.apcatb.2013.12.036.

References

[1] K. Ballschmiter, Pure Appl. Chem. 68 (9) (1996) 1771–1780.
[2] A. Ghosh, M. Khurana, A. Chauhan, M. Takeo, A.K. Chakraborti, R.K. Jain, Environ. Sci. Technol. 44 (3) (2010) 1069–1077.
[3] S.J. Rosser, A. Basran, E.R. Travis, C.E. French, N.C. Bruce, Adv. Appl. Microbiol. 49 (2001) 1–35.
[4] Y. Jiang, J. Wen, J. Bai, X. Ji, Z. Hu, J. Hazard. Mater. 147 (2007) 672–676.
[5] G. Annadurai, R.S. Juang, D.J. Lee, Waste Manage. 22 (2002) 703–710.
[6] J.F. Novotny, D. Strout, Can. J. Microbiol. 36 (8) (1990) 557–560.
[7] K. Rajeshwar, J.G. Ibanez, Environmental Electrochemistry, Academic Press, San Diego, 1997, pp. 361–497.
[8] G. Laera, D. Cassano, A. Lopez, A. Pinto, A. Pollice, G. Ricco, G. Mascolo, Environ. Sci. Technol. 46 (2) (2012) 1010–1018.
[9] M.A. Rauf, S.S. Ashraf, Chem. Eng. J. 151 (2009) 10–18.
[10] J.H. Carey, Water Pollut. Res. J. Can. 27 (1992) 1–21.
[11] R. Munter, Proc. Estonian Acad. Sci. Chem. 50 (2) (2001) 59–80.
[12] S. Maddila, V.D.B.C. Dasireddy, S.B. Jonnalagadda, Appl. Catal. B: Environ. 138–139 (2013) 149–160.
[13] M.E. Lovato, C.A. Martin, A.E. Cassano, Chem. Eng. J. 46 (3) (2009) 486–497.
[14] P. Ormad, S. Cortes, A. Puig, J.L. Ovelleiro, Water Res. 31 (9) (1997) 2387–2391.
[15] J. Hoigne, H. Bader, Water Res. 10 (1976) 377–386.
[16] A. Rahman, V.S.R. Pullabhotla, S.B. Jonnalagadda, Catal. Commun. 9 (2008) 2417–2421.
[17] S.B. Jonnalagadda, V.S.R. Pullabhotla, S. Maddila, E.C. Chetty, Int. J. Chem. 1 (1) (2012) 119–129.
[18] M. Trapido, A. Hirvonen, Y. Veressinina, J. Hentunen, R. Munter, Ozone Sci. Eng. 19 (1997) 75–96.
[19] L. Khachatryan, B. Dellinger, Environ. Sci. Technol. 45 (21) (2011) 9232–9239.
[20] H. Liu, P. Zhang, Y. Wang, B. Yang, J. Shu, Environ. Sci. Technol. 46 (24) (2012) 13262–13269.
[21] W.H. Glaze, J.W. Kang, D.H. Chapin, Ozone Sci. Eng. 9 (1997) 335–352.
[22] S. Maddila, V.D.B.C. Dasireddy, E.O. Oseghe, S.B. Jonnalagadda, Appl. Catal. B: Environ. 142–143 (2013) 129–141.
[23] E.C. Chetty, S. Maddila, C. Southway, S.B. Jonnalagadda, Ind. Eng. Chem. Res. 51 (2012) 2864–2873.
[24] V.S.R.R. Pullabhotla, S.B. Jonnalagadda, Ind. Eng. Chem. Res. 48 (20) (2009) 9097–9105.
[25] J. Liu, Q. Sun, Y. Fu, H. Zhao, A. Auroux, J. Shen, Catal. Lett. 126 (2008) 155–163.
[26] D.R. Malini, C. Sanjeeviraj, Electrochim. Acta 104 (2013) 162–169.
[27] T. Hirata, A. Watanabe, J. Solid State Chem. 158 (2001) 254–261.
[28] E.C. Chetty, V.B. Dasireddy, S. Maddila, S.B. Jonnalagadda, Appl. Catal. B: Environ. 117–118 (2012) 18–28.
[29] J.J. Zuckerman, A.D. Norman, B.C. Gates, Metal Oxide Supports in Inorganic Reactions and Methods: Reactions Catalyzed by Inorganic Compounds, John Wiley & Sons, Inc., Hoboken, NJ, 2007, 16.
[30] A. Corma, H. Garcia, Chem. Soc. Rev. 37 (2008) 2096–2126.
[31] A. Zaera, J. Phys. Chem. Lett. 1 (3) (2010) 621–627.
[32] A. Sirijaruphan, J.G. Goodwin Jr., R.W. Rice, D. Wei, K.R. Butcher, G.W. Roberts, J.J. Spiv, Appl. Catal. A: Gen. 281 (2005) 11–18.
[33] M. Okumura, S. Nakamura, S. Tsubota, T. Nakamura, M. Azuma, M. Haruta, Catal. Lett. 51 (1998) 53–58.